Author Manuscript

Author Manuscript

Author Manuscript

Author Manuscript

HHS Public Access

Author manuscript

Adv Mater. Author manuscript; available in PMC 2020 June 01.

Published in final edited form as:

Adv Mater. 2019 June ; 31(23): e1900192. doi:10.1002/adma.201900192.

Photothermal Therapy Promotes Tumor Infiltration and Antitumor Activity of CAR T Cells

Qian Chen,
Department of Bioengineering, California NanoSystems Institute, Jonsson Comprehensive Cancer Center and Center for Minimally Invasive Therapeutics, University of California, Los Angeles, CA 90095, United States

Joint Department of Biomedical Engineering, University of North Carolina at Chapel Hill and North Carolina State University, Raleigh, NC 27695, USA

Jiangsu Key Laboratory for Carbon-Based Functional Materials and Devices, Institute of Functional Nano and Soft Materials (FUNSOM), Soochow University, 199 Ren'ai Road, Suzhou 215123, Jiangsu, P.R. China

Quanyin Hu,
Department of Bioengineering, California NanoSystems Institute, Jonsson Comprehensive Cancer Center and Center for Minimally Invasive Therapeutics, University of California, Los Angeles, CA 90095, United States

Joint Department of Biomedical Engineering, University of North Carolina at Chapel Hill and North Carolina State University, Raleigh, NC 27695, USA

Elena Dukhovlinova,
Lineberger Comprehensive Cancer Center, University of North Carolina, Chapel Hill, North Carolina 27599, United States

Guojun Chen,
Department of Bioengineering, California NanoSystems Institute, Jonsson Comprehensive Cancer Center and Center for Minimally Invasive Therapeutics, University of California, Los Angeles, CA 90095, United States

Sarah Ahn,
Lineberger Comprehensive Cancer Center, University of North Carolina, Chapel Hill, North Carolina 27599, United States

Chao Wang,
Joint Department of Biomedical Engineering, University of North Carolina at Chapel Hill and North Carolina State University, Raleigh, NC 27695, USA

[*]Corresponding author. guzhen@ucla.edu, gdotti@med.unc.edu.

Conflict of Interest
The authors declare no conflict of interest.

Supporting Information Supporting Information is available from the Wiley Online Library or from the author.

Author Manuscript Author Manuscript Author Manuscript Author Manuscript

Jiangsu Key Laboratory for Carbon-Based Functional Materials and Devices, Institute of Functional Nano and Soft Materials (FUNSOM), Soochow University, 199 Ren'ai Road, Suzhou 215123, Jiangsu, P.R. China

Frances S. Ligler,
Joint Department of Biomedical Engineering, University of North Carolina at Chapel Hill and North Carolina State University, Raleigh, NC 27695, USA

Gianpietro Dotti*,
Lineberger Comprehensive Cancer Center, University of North Carolina, Chapel Hill, North Carolina 27599, United States

Zhen Gu*
Department of Bioengineering, California NanoSystems Institute, Jonsson Comprehensive Cancer Center and Center for Minimally Invasive Therapeutics, University of California, Los Angeles, CA 90095, United States

Joint Department of Biomedical Engineering, University of North Carolina at Chapel Hill and North Carolina State University, Raleigh, NC 27695, USA

Abstract

Chimeric antigen receptor (CAR)-redirected T lymphocytes (CAR T cells) show modest therapeutic efficacy in solid tumors. The desmoplastic structure of the tumor and the immunosuppressive tumor microenvironment usually account for the reduced efficacy of CAR T cells in solid tumors. Mild hyperthermia of the tumor reduces its compact structure and interstitial fluid pressure (IFP), increases blood perfusion, releases antigens and promotes the recruitment of endogenous immune cells. Therefore, the combination of mild hyperthermia with the adoptive transfer of CAR T cells could potentially increase the therapeutic index of these cells in solid tumors. We found that the chondroitin sulfate proteoglycan-4 (CSPG4)-specific CAR T cells infused in Nod scid gamma (NSG) mice engrafted with the human melanoma WM115 cell line had superior antitumor activity after photothermal ablation of the tumor. Our findings suggest that photothermal therapy facilitates the accumulation and effector function of CAR T cells within the solid tumor.

Graphical Abstract

Author Manuscript Author Manuscript Author Manuscript Author Manuscript

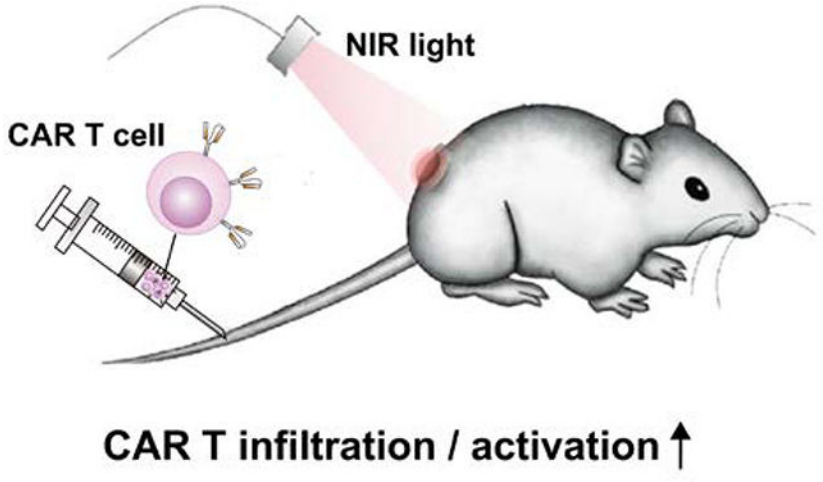

Photothermal ablation of tumors is demonstrated to promote the therapeutic efficacy of CAR T cells. Mild hyperthermia can promote direct tumor cell killing, partially disrupt the extracellular matrix, decrease the interstitial fluid pressure and increase local blood perfusion. All these modifications caused by photothermal therapy ultimately promote the infiltration and antitumor effects of adoptively transferred CAR T cells.

Keywords

CAR T cells; photothermal therapy; immunotherapy; cell therapy; drug delivery

T cells genetically engineered with chimeric antigen receptor (CAR) provide radically innovative and sophisticated methods for cancer treatment [1]. CARs are typically composed of the antigen-targeting region of a monoclonal antibody fused to the signaling molecules of the T cell receptor and costimulatory molecules [2]. CD19-specific CAR T cells have been approved by Food and Drug Administration (FDA) to treat B cell malignancies [3]. However, the efficacy of CAR T cells against solid tumors remains modest mostly because of the inefficient infiltration of CAR T cells into the tumor and the abundant presence of immunosuppressive cells in the tumor [4]. To exploit their effector function, CAR T cells must engage chemotactic signals to traffic and accumulate into the tumor [5]. The physical barriers represented by the extracellular matrix and stroma, together with the abnormal tumor vasculature and high interstitial fluid pressure (IFP), prevent the adequate infiltration of CAR T cells [6]. The development of strategies to promote the infiltration of CAR T cells in solid tumors has become one of the major themes in the field.

Photothermal therapy employs optical absorbing agents to ‘burn’ tumor cells by effectively generating heat under the near-infrared (NIR) light irradiation [7]. Compared to traditional cancer therapies, photothermal therapy has unique advantages that include high selectivity, low systemic toxicity and limited therapeutic resistance [8]. As shown in Figure 1, we propose that poly(lactic-co-glycolic) acid (PLGA) nanoparticles [9] loaded with indocyanine green (ICG) [7a, 10], a NIR dye used as the photothermal agent, injected intratumorally can promote direct tumor cell killing, partial disruption of the extracellular matrix, decrease of

Author Manuscript Author Manuscript Author Manuscript Author Manuscript

the IFP and increase of the blood perfusion [11]. Moreover, the destruction of cancer cells by hyperthermia causes inflammation, which could enhance recruitment of immune cells and secretion a variety of chemokines and cytokines. Working together with the released tumor-specific antigens after photothermal ablation, the proposed therapy greatly enhances the tumor infiltration and activation of CAR T cells and improves efficacy.

PLGA, a polymer applied in US FDA-approved formulations, was used to encapsulate ICG *via* an oil-in-water (o/w) emulsion method. Monodispersed PLGA-ICG nanoparticles (~ 100 nm) with spherical shape were obtained, as revealed by the transmission electron microscope (TEM) imaging and dynamic light scattering (DLS) (Figure 2a). PLGA-ICG nanoparticles exhibited a characteristic absorption peak of ICG at ~780 nm, which is ideal for effective photothermal therapy (Figure 2b). Temperature elevation was observed when the PLGA-ICG suspension was irradiated using the 808 nm laser (0.5 W/cm^2 for 5 min), while pure phosphate buffered saline (PBS) solution showed modest temperature increase under the same laser irradiation (Figure 2c and d, Figure S1). Confocal fluorescent images of propidium iodide (PI) and Calcine AM co-stained cells and the PI and Annexin V staining with flow cytometry further confirmed the effective photothermal ablation of cancer cells (Figure S2).

We then investigated whether *ex vivo* photothermal exposure of the tumor cells affects CAR T cell functions. To demonstrate this proof of concept, we used CAR T cells targeting the antigen chondroitin sulfate proteoglycan-4 (CSPG4) that is overexpressed in melanoma and glioblastoma, while limited distribution is observed in normal tissues [12]. T lymphocytes obtained from healthy donors were engineered to express the CSPG4.CAR (Figure S3). We evaluated the proliferation of CAR.$CSPG4^+$ T cells using the carboxyfluorescein diacetate succinimidyl ester (CFSE)-based assay. The melanoma cell line WM115 that expresses CSPG4 with or without photothermal exposure, was placed in the upper chamber of a transwell with the pore size ~ 1μm and CAR.$CSPG4^+$ T cells were seeded in the lower chamber. After three days of culture, CSPG4.CAR T cells vigorously proliferated after coculture with WM115 cells upon photothermal ablation, suggesting that the CSPG4 protein released from WM115 cells after photothermal therapy engages and stimulates CSPG4-specific CAR T cells (Figure 2e and f). The activation of CSPG4.CAR T cells in response to WM115 cells after photothermal ablation was further confirmed by the increased production of interleukin-2 (IL-2) and interferon-γ (IFN-γ) (Figure 2g and h).

To validate whether the photothermal therapy can enhance the antitumor effects of CAR T cells in solid tumors, we first characterized the effects of mild photothermal ablation in NSG mice bearing the human melanoma WM115 tumor subcutaneously. We injected intratumorally the PLGA-ICG nanoparticles and irradiated the tumor with the 808 nm laser at the power density of 0.3 W/cm^2. The temperature of the tumor injected with PLGA-ICG increased to ~ 44 ^oC within 2 minutes as monitored by an infrared thermal camera (Figure 3a and b). After the photothermal treatment, the morphology of the tumor vasculature appeared dilated with reduced IFP as compared to control tumors (Figure 3c). Increased ultrasonic signal was also recorded 24 hours after the photothermal ablation by ultrasound imaging with a microbubble contrast agent, further suggesting an increase in tumor perfusion (Figure 3d). Moreover, the signals of the hypoxia probe pimonidazole and the

Author Manuscript Author Manuscript Author Manuscript Author Manuscript

hypoxia-inducible factor (HIF)-1α were decreased, suggesting enhanced oxygenation (Figure 3e). Finally, photothermal ablation caused the intratumor increase of murine monocytes ($CD45^+CD11b^+$) and dendritic cells ($CD45^+CD11c^+$) (Figure 3f–h) as well as murine chemokines such as chemokine ligand 5 (CCL5), CCL 11, chemokine (C-X-C motif) ligand 1 (CXCL1), CCL 2, CCL 3, and CCL 4 (Figure 3i).

Next, a xenograft model of melanoma was established by inoculating WM115 tumor cells into both flanks of NSG mice. After three weeks, the tumors in the right flank were intratumorally injected with PLGA-ICG and irradiated with the 808 nm laser. Two hours later, 1×10^7 CAR.$CSPG4^+$ T cells or CAR.$CD19^+$ T cells labeled with the firefly luciferase were intravenously injected. T cell biodistribution was monitored by *in vivo* imaging system (IVIS) at different time points after CAR T cell administration. Increased localization of CAR.$CSPG4^+$ T cells was observed in tumors that received photothermal therapy as compared to the contralateral tumors (Figure S4, Figure 4a and b). Flow cytometry (Figure 4c–f) and immunofluorescence imaging (Figure 4g) confirmed the accumulation of CAR.$CSPG4^+$ T cells in the tumors treated with photothermal therapy.

To assess the antitumor activity of combining photothermal therapy and CAR.$CSPG4^+$ T cells, we labeled the WM115 human melanoma tumor cell line with firefly luciferase. WM115 tumor bearing mice were intratumorally injected with PLGA-ICG and irradiated with the 808 nm laser for 20 minutes at a power density of 0.3 W/cm^2. Two hours later, 1×10^7 CAR.$CSPG4^+$ T cells were intravenously injected into the mice. Tumor growth was monitored using both *in vivo* bioluminescence (Figure 5a) and caliper measurement (Figure 5b and c). Photothermal therapy combined with CAR.$CSPG4^+$ T cells significantly suppressed the tumor growth up to 20 days as compared with control groups. Two out of six mice receiving the combined treatment were macroscopically tumor free at the end of the experiment as confirmed by immunohistochemistry and terminal deoxynucleotidyl transferase-mediated dUTP-biotin nick end labeling assay (Figure S5 and Figure S6). In parallel experiments, we measured cytokine levels in treated mice. Murine IL-6 was increased after photothermal therapy (Figure 5d). Moreover, human IL-2 and IFN-γ released by CAR T cells were also significantly increased, especially in the mice receiving the combined treatment (Figure 5e and f).

In summary, mild heating of the tumor triggers physicochemical and physiological changes of the tumor, resulting in increased infiltration and accumulation of CAR.$CSPG4^+$ T cells. In addition to directly killing tumor cells, mild heating can also partially destroy tumor cells and extracellular matrix, thereby reducing the density of the solid tumor and IFP and expanding tumor blood vessels. Moreover, tumor-associated antigens released from photothermal therapy may burst endogenous immune cells and activate the immune system and potentially control metastatic lesions[10, 13]. Facilitated by the photothermal therapy, CAR.$CSPG4^+$ T lymphocytes traffic to and accumulate at the tumor site, following the chemokine and antigen attraction. In NSG mice engrafted with the human melanoma WM115 tumors, effective therapeutic effect was achieved after mild heating of solid tumors (~ 44 °C) and subsequently intravenous infusion of CAR.$CSPG4^+$ T cells. Thus, the proposed combination provides a promising platform to increase the therapeutic index of CAR T cells in solid tumors simply and safely. The proposed platform may be further

Author Manuscript Author Manuscript Author Manuscript Author Manuscript

potentiated by tuning treatment variables including duration and frequency of the photothermal and by including targeted immunomodulatory therapeutics.

Experimental Section

Materials, cell lines, and animals

All chemicals were obtained from Sigma-Aldrich and used without any purification. Human melanoma WM115 cells and WM115-luc cells were obtained from Dr. Gianpietro Dotti at UNC and cultured in RPMI 1640 (HyClon) medium containing 10% heat inactivated fetal calf serum (F Invitrogen, Carlsbad, CA), 2 mmol/L GlutaMAX (Invitrogen), 200 IU/mL penicillin, and 200 mg/mL streptomycin (Invitrogen) in an incubator at 37 °C in 5% CO_2. The CD19-specific CAR T lymphocytes and CSPG4-specific CAR T lymphocytes also were generated in Dr. Gianpietro Dotti's lab at UNC[12b]. CAR T cells were cultured and expanded in complete medium containing 45% RPMI 1640 and 45% Click's medium (Irvine Scientific) with 10% FCS (HyClone), 2 mmol/L GlutaMAX, 100 IU/mL penicillin, and 100 mg/mL streptomycin. Cells were fed twice a week with recombinant interleukin-7 (IL-7, 5 ng/mL; Pepro Tech, Inc.) and interleukin-15 (IL-15) (10 ng/mL; Pepro Tech, Inc.). Female NSG mice (6–10 weeks) were purchased from Jackson Lab. All mouse studies were carried out following the protocols approved by the Institutional Animal Care and Use Committee at the University of North Carolina at Chapel Hill and North Carolina State University and complied with all relevant ethical regulations.

Synthesis and characterization of PLGA-ICG nanoparticles

PLGA-ICG nanoparticles were prepared using an o/w single-emulsion method[10]. Briefly, photothermal agent ICG was dissolved in DMSO at 10 mg/ml, and then added to PLGA dichloromethane solution. The mixture was homogenized with 5% w/v PVA solution by Selecta Sonopuls for 10 min. Then, the emulsion was added to additional 5% w/v solution of PVA to evaporate the organic solvent. PLGA-ICG nanoparticles were obtained after centrifugation at 3,500g for 20 min. The morphology of PLGA-ICG nanoparticles was characterized by transmission electron microscopy (TEM, JEOL 2000FX), and the size distribution was measured by the Zetasizer Nano-ZS (Malvern Instruments, UK). The absorbance spectrum was recorded by Nanodrop.

Cellular experiments

To study the proliferation the CAR.CSPG4$^+$ T lymphocytes, CAR.CSPG4$^+$ T lymphocytes (1×10^6 cells) were stained with carboxyfluorescein succinimidyl ester (CFSE, 5 μM) according to the protocol of the Cell Trace™ CFSE Cell Proliferation Kit (Invitrogen). Then, CAR.CSPG4$^+$ T lymphocytes were incubated with PLGA-ICG nanoparticle solution after photothermal ablation, WM115 cells or WM115 cells after photothermal ablation using a transwell system (400 μm) for 3 days in the incubator. The fluorescent intensity of CFSE was detected by flow cytometry to monitor the proliferation of T cells. Meanwhile, the medium supernatant of CAR.CSPG4$^+$ T lymphocytes was collected and the different cytokines including IL-2 and IFN-γ were measured by an enzyme-linked immunosorbent assay (ELISA).

Author Manuscript Author Manuscript Author Manuscript Author Manuscript

In vivo tumor models and treatment

For the *in vivo* biodistribution of CAR.CSPG4$^+$ T lymphocytes, 5×10^6 WM115 human melanoma cells were subcutaneously injected into both sides of each mouse. After ~20 days, when the tumor volume reached ~100 mm^3, PLGA-ICG nanoparticles were intratumorally injected into the right-side tumors and irradiated with an 808 nm laser at the power density of 0.3 W/cm^2 for 20 min. Two hours later, 1 × 10^7 CAR.CSPG4$^+$ T lymphocytes labeled with luciferase were intravenously injected into the mice. Different time points after intravenous injection of T cells, mice were imaged *via* an IVIS Spectrum Imaging System (Perkin Elmer Ltd) for 1 min to monitor the biodistribution of T cells.

For *in vivo* combination therapy, NSG mice bearing subcutaneous fLuc-WM115 tumors were divided into four groups (n=6 per group): (a) untreated; (b) intratumorally injected with PLGA-ICG nanoparticles and irradiated by the 808-nm laser (0.3 W/cm^2, 10 min); (c) intravenously injected with 1 × 10^7 CAR.CSPG4$^+$ T lymphocytes only; (d) intratumorally injected with PLGA-ICG nanoparticles and irradiated by the 808-nm laser (0.3 W/cm^2, 10 min), and then intravenously injected with 1 × 10^7 CAR.CSPG4$^+$ T lymphocytes. The changes of the temperature on the surface of tumor were monitored by an IR thermal camera. The tumor sizes were recorded by a digital caliper every 2 days and calculated according to the following formula: width^2 × length × 0.5. The tumor was also monitored using an *in vivo* bioluminescence imaging system. Ten minutes after intraperitoneal injection of d-luciferin (Thermo Scientific™ Pierce™, 150 mg/kg) into each mouse, mice were imaged *via* an IVIS Spectrum Imaging System for 1 s.

Supplementary Material

Refer to Web version on PubMed Central for supplementary material.

Acknowledgements

This work was supported by grants from the Jonsson Comprehensive Cancer Center at UCLA, the Alfred P. Sloan Foundation (Sloan Research Fellowship) and NC TraCS, the NIH Clinical and Translational Science Awards (CTSA, NIH grant 1L1TR001111) at UNC, and a pilot grant from the UNC Cancer Center to Z.G, and the NCI of NIH (T32CA196589, R25NS094093).

Reference

[1]. aHinrichs CS, Rosenberg SA, Immunol. Rev 2014, 257, 56–71; [PubMed: 24329789] bPhilip B, Kokalaki E, Mekkaoui L, Thomas S, Straathof K, Flutter B, Marin V, Marafioti T, Chakraverty R, Linch D, Blood 2014, blood-2014–2001-545020;cHinrichs CS, Restifo NP, Nat. Biotechnol 2013, 31, 999. [PubMed: 24142051]

[2]. aKochenderfer JN, Dudley ME, Feldman SA, Wilson WH, Spaner DE, Maric I, Stetler-Stevenson M, Phan GQ, Hughes MS, Sherry RM, Blood 2012, 119, 2709–2720; [PubMed: 22160384] bSavoldo B, Ramos CA, Liu E, Mims MP, Keating MJ, Carrum G, Kamble RT, Bollard CM, Gee AP, Mei Z, J. Clin. Invest 2011, 121, 1822–1826; [PubMed: 21540550] cBrentjens RJ, Rivière I, Park JH, Davila ML, Wang X, Stefanski J, Taylor C, Yeh R, Bartido S, Borquez-Ojeda O, Blood 2011, blood-2011–2004-348540.

[3]. aMaude SL, Laetsch TW, Buechner J, Rives S, Boyer M, Bittencourt H, Bader P, Verneris MR, Stefanski HE, Myers GD, New Engl. J. Med 2018, 378, 439–448; [PubMed: 29385370] bNeelapu SS, Locke FL, Bartlett NL, Lekakis LJ, Miklos DB, Jacobson CA, Braunschweig I, Oluwole OO, Siddiqi T, Lin Y, New Engl. J. Med 2017, 377, 2531–2544; [PubMed: 29226797]

Author Manuscript Author Manuscript Author Manuscript Author Manuscript

cDavila ML, Riviere I, Wang X, Bartido S, Park J, Curran K, Chung SS, Stefanski J, Borquez-Ojeda O, Olszewska M, Sci. Transl. Med 2014, 6, 224ra225–224ra225.

[4]. aFeig C, Jones JO, Kraman M, Wells RJ, Deonarine A, Chan DS, Connell CM, Roberts EW, Zhao Q, Caballero OL, Proc. Natl. Acad. Sci. U.S.A 2013, 110, 20212–20217; [PubMed: 24277834] bMaus MV, Haas AR, Beatty GL, Albelda SM, Levine BL, Liu X, Zhao Y, Kalos M, June CH, Cancer Immunol. Res 2013;cMoon EK, Wang L-C, Dolfi DV, Wilson CB, Ranganathan R, Sun J, Kapoor V, Scholler J, Puré E, Milone MC, Clin. Cancer Res 2014;dNewick K, O'Brien S, Moon E, Albelda SM, Annu. Rev. Med 2017, 68, 139–152. [PubMed: 27860544]

[5]. aParish CR, Nat. Rev. Immunol 2006, 6, 633; [PubMed: 16917509] bMuller WA, Trends Immunol 2003, 24, 326–333;cAdusumilli PS, Cherkassky L, Villena-Vargas J, Colovos C, Servais E, Plotkin J, Jones DR, Sadelain M, Sci. Transl. Med 2014, 6, 261ra151–261ra151.

[6]. aCaruana I, Savoldo B, Hoyos V, Weber G, Liu H, Kim ES, Ittmann MM, Marchetti D, Dotti G, Nat. Med 2015, 21, 524; [PubMed: 25849134] bJain RK, Stylianopoulos T, Nat. Rev. Clin. Oncol 2010, 7, 653; [PubMed: 20838415] cStylianopoulos T, Martin JD, Chauhan VP, Jain SR, Diop-Frimpong B, Bardeesy N, Smith BL, Ferrone CR, Hornicek FJ, Boucher Y, Proc. Natl. Acad. Sci. U.S.A 2012, 201213353.

[7]. aChen Q, Liang C, Wang C, Liu Z, Adv. Mater 2015, 27, 903–910; [PubMed: 25504416] bChen Q, Ke H, Dai Z, Liu Z, Biomaterials 2015, 73, 214–230; [PubMed: 26410788] cCheng L, Wang C, Feng L, Yang K, Liu Z, Chem. Rev 2014, 114, 10869–10939; [PubMed: 25260098] dRobinson JT, Tabakman SM, Liang Y, Wang H, Sanchez Casalongue H, Vinh D, Dai H, J. Am. Chem. Soc 2011, 133, 6825–6831. [PubMed: 21476500]

[8]. aYang K, Zhang S, Zhang G, Sun X, Lee S-T, Liu Z, Nano Lett 2010, 10, 3318–3323; [PubMed: 20684528] bChen Q, Wang C, Zhan Z, He W, Cheng Z, Li Y, Liu Z, Biomaterials 2014, 35, 8206–8214. [PubMed: 24957292]

[9]. Makadia HK, Siegel SJ, Polymers 2011, 3, 1377–1397. [PubMed: 22577513]

[10]. Chen Q, Xu L, Liang C, Wang C, Peng R, Liu Z, Nat. Commun 2016, 7, 13193. [PubMed: 27767031]

[11]. aSong G, Liang C, Gong H, Li M, Zheng X, Cheng L, Yang K, Jiang X, Liu Z, Adv. Mater 2015, 27, 6110–6117; [PubMed: 26331476] bCheng L, Yuan C, Shen S, Yi X, Gong H, Yang K, Liu Z, ACS Nano 2015, 9, 11090–11101; [PubMed: 26445029] cStapleton S, Dunne M, Milosevic M, Tran CW, Gold MJ, Vedadi A, Mckee TD, Ohashi PS, Allen C, Jaffray DA, ACS Nano 2018, 12, 7583–7600. [PubMed: 30004666]

[12]. aPluschke G, Vanek M, Evans A, Dittmar T, Schmid P, Itin P, Filardo EJ, Reisfeld RA, Proc. Natl. Acad. Sci. U.S.A 1996, 93, 9710–9715; [PubMed: 8790396] bGeldres C, Savoldo B, Hoyos V, Caruana I, Zhang M, Yvon E, Del Vecchio M, Creighton CJ, Ittmann M, Ferrone S, Clin. Cancer Res 2014, 20, 962–971; [PubMed: 24334762] cWang X, Katayama A, Wang Y, Yu L, Favoino E, Sakakura K, Favole A, Tsuchikawa T, Silver S, Watkins SC, Cancer Res. 2011, canres. 1134.2010;dMorello A, Sadelain M, Adusumilli PS, Cancer Discov. 2016, 6, 133–146; [PubMed: 26503962] eRivera Z, Ferrone S, Wang X, Jube S, Yang H, Pass HI, Kanodia S, Gaudino G, Carbone M, Clin. Cancer Res 2012, clincanres. 0628.2012.

[13]. Wang C, Xu L, Liang C, Xiang J, Peng R, Liu Z, Adv. Mater 2014, 26, 8154–8162. [PubMed: 25331930]

Author Manuscript
Author Manuscript
Author Manuscript
Author Manuscript

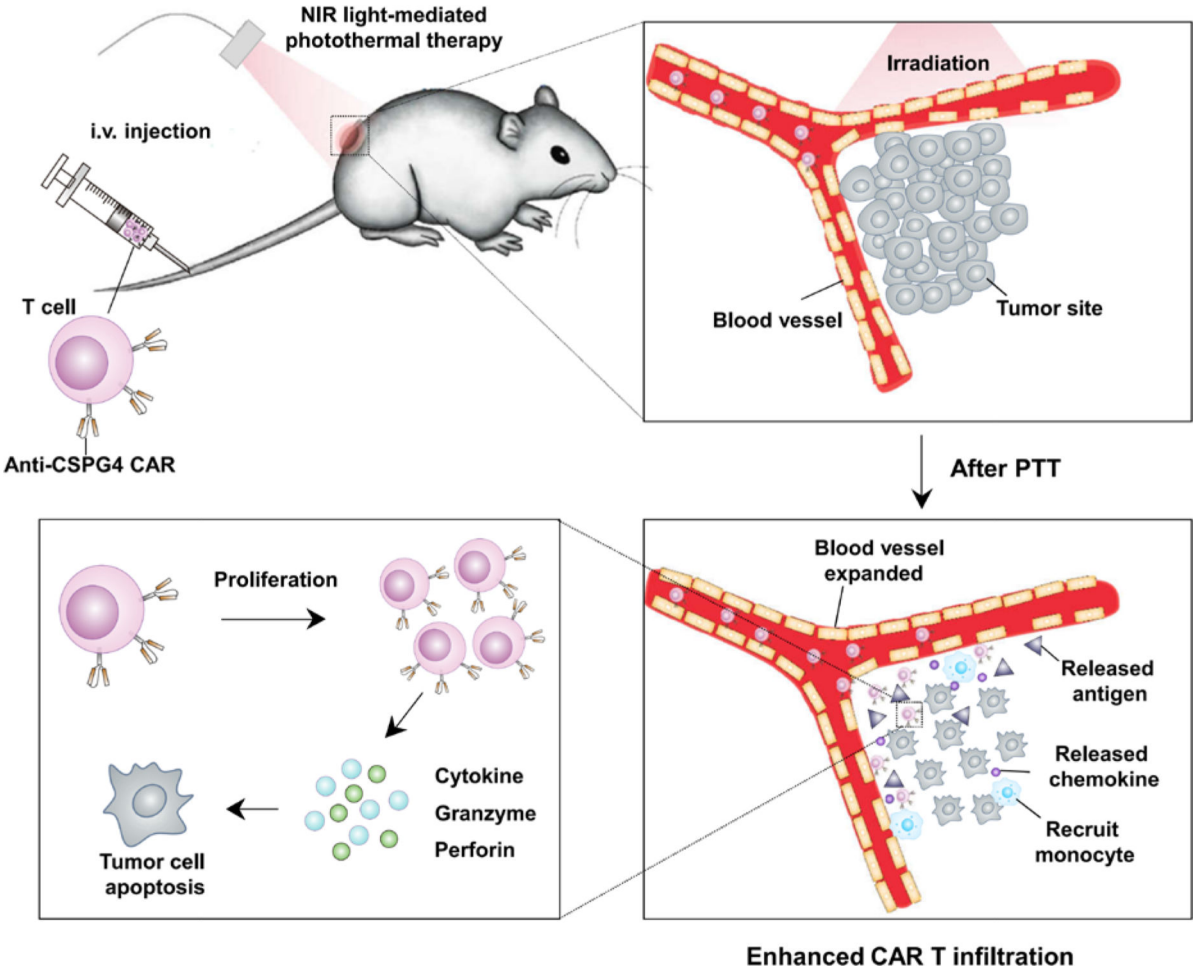

Figure 1.

Schematic illustration showing the effects of the mild heating of the tumor that causes enhanced infiltration and activation of adoptive transfer CAR.CSPG4^{+} T cells.

Author Manuscript Author Manuscript Author Manuscript Author Manuscript

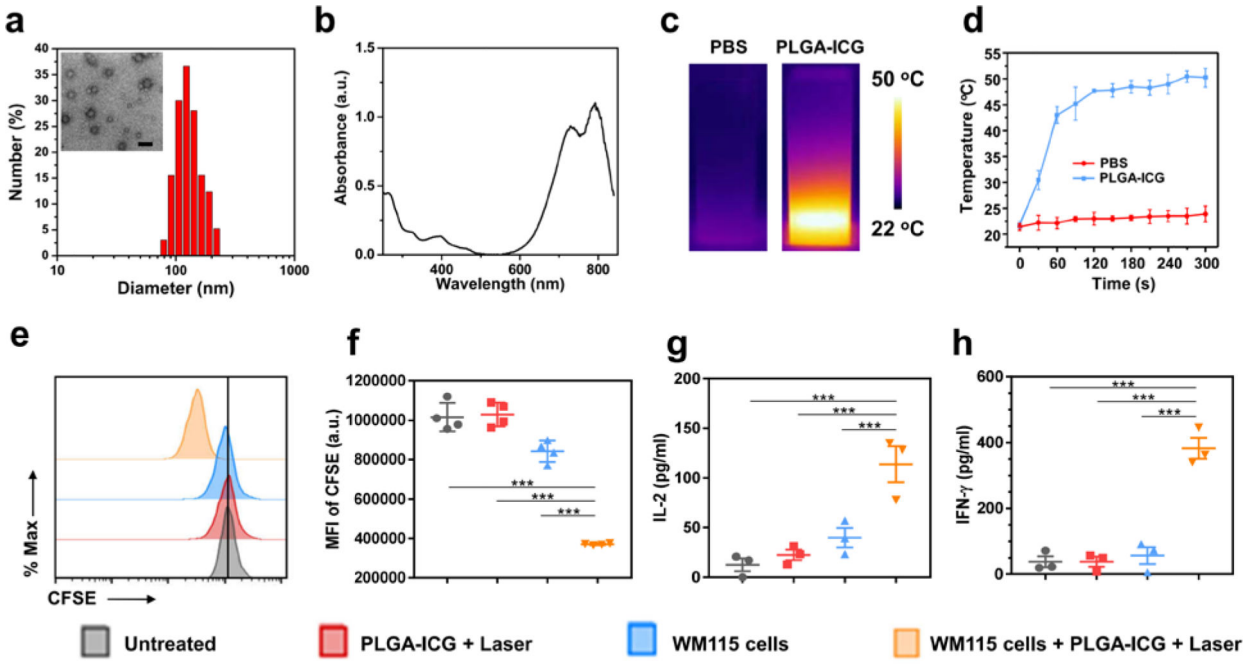

Figure 2. Photothermal therapy of the tumor promotes CAR T cell proliferation and cytokine release.

(a) Hydrodynamic diameter of PLGA-ICG nanoparticles measured by dynamic light scattering. Insert is the TEM image of PLGA-ICG (Scale bar, 200 nm). (b) The UV–vis–NIR spectrum of PLGA-ICG, exhibiting high absorption in the near infrared region. (c & d) IR thermal images (c) and temperature curves (d) of PBS and PLGA-ICG under the 808-nm light irradiation for 5 min at the power density of 0.5 W/cm^2. Data are presented as mean ± s.e.m. (n=3) (e) Representative flow cytometry analysis of CAR.CSPG4$^+$ T cells labeled with CFSE three days after the indicated treatments. (f) Mean fluorescence intensity of CFSE, indicating T cell proliferation. Data are presented as mean ± s.e.m. (n=4). (g & h) Detection of IL-2 (g) and IFN-γ (h) in the supernatant of CAR.CSPG4$^+$ T cells, three days after the indicated treatments. Data are presented as mean ± s.e.m. (n=4). Statistical significance was calculated *via* one-way ANOVA with a Tukey post-hoc test. P value: *P < 0.05; **P < 0.01; ***P < 0.001.

Author Manuscript Author Manuscript Author Manuscript Author Manuscript

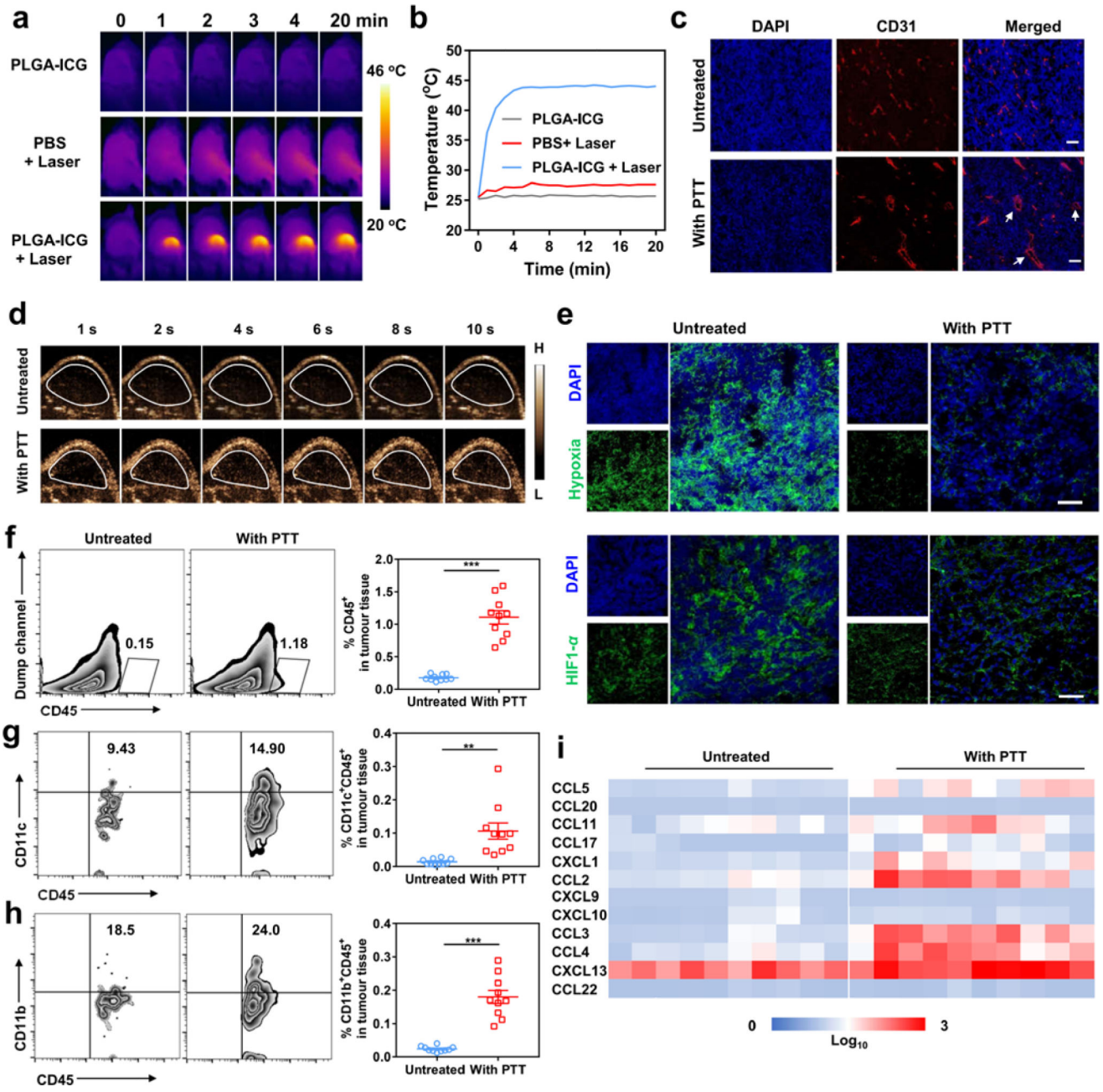

Figure 3. Photothermal therapy of the tumor modifies the tumor microenvironment.

(a) IR thermal images of WM115-tumor-bearing mice injected with PLGA-ICG or PBS with the 808 nm laser irradiation (0.3 W/cm^2, 20 min). (b) Changes of the tumor temperature measured by the IR thermal imaging. (c) Immunofluorescence imaging of tumors collected from mice 24 hours after photothermal therapy. Scale bar, 50 μm. (d) Ultrasound imaging illustrating the blood perfusion of the WM115 tumors. Microbubbles injected intravenously were used as the ultrasound contrast agent. (e) Representative hypoxia and HIF1-α immunofluorescence staining of the tumors after photothermal therapy (Scale bar, 50 μm). (f) Representative flow cytometry plots and quantification of murine CD45$^+$ cells infiltrating the tumor after photothermal therapy. Data are presented as mean ± s.e.m. (n=10). (g & h)

Author Manuscript Author Manuscript Author Manuscript Author Manuscript

Representative flow cytometry plot and quantification of murine $CD11c^+$ (g) and $CD11b^+$ (h) cells gating on $CD45^+$ cells. Data are presented as mean ± s.e.m. (n=10). (i) Quantification of chemokines in the tumor (n=10). Statistical significance was calculated *via* two-tailed Student's t-test. P value: *$P < 0.05$; **$P < 0.01$; ***$P < 0.001$.

Author Manuscript Author Manuscript Author Manuscript Author Manuscript

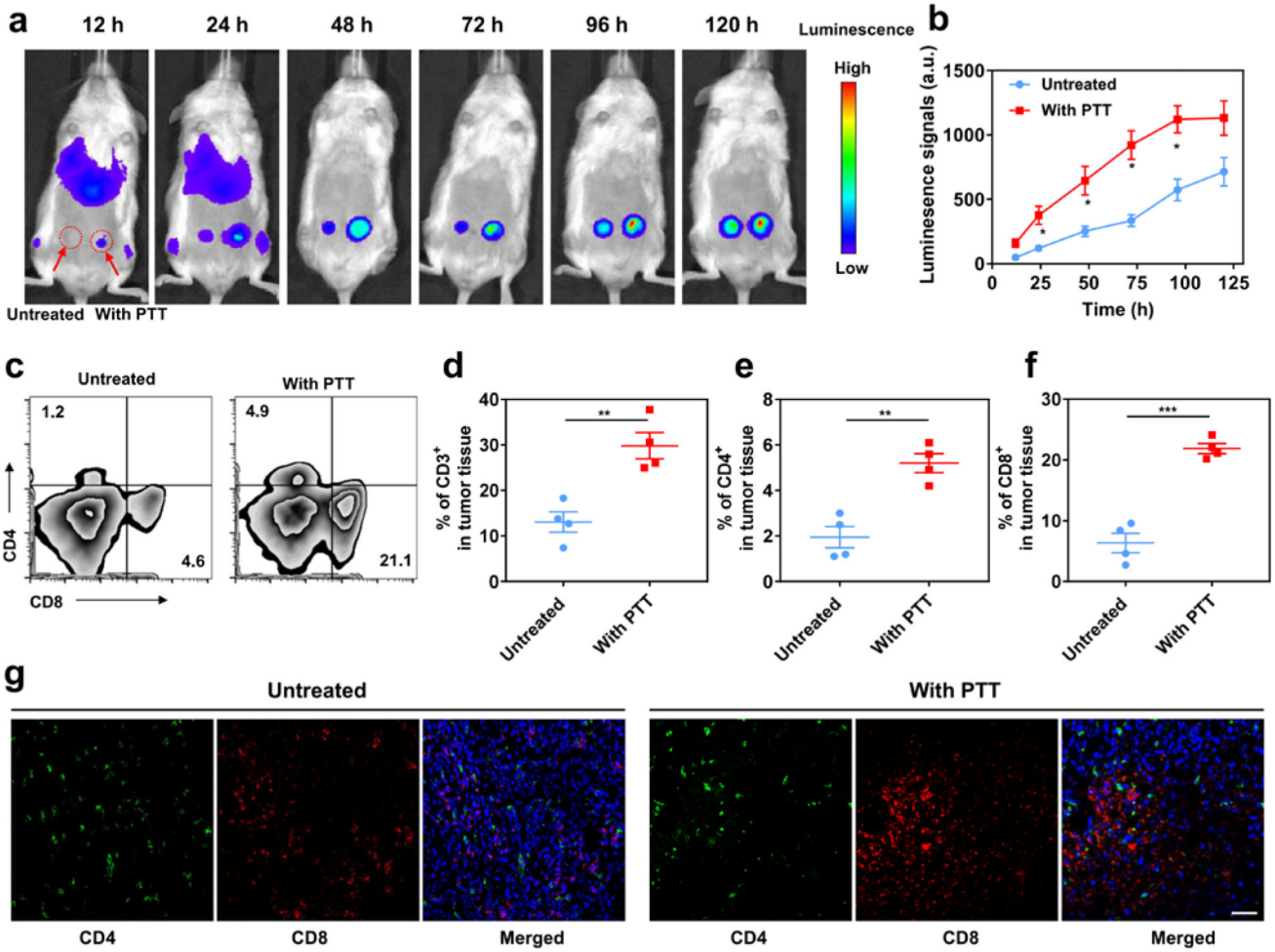

Figure 4. Photothermal ablation of the tumor increases the infiltration of adoptively transferred CAR T cells.

(a) *In vivo* bioluminescence imaging of the CAR.CSPG4$^+$ T cells. (b) Quantification of CAR.CSPG4$^+$ T cells detected in the tumor with or without photothermal ablation. Data are presented as mean ± s.e.m. (n=3). (c) Representative flow cytometry plots of CAR.CSPG4$^+$ T cells infiltrating the tumor. (d-e) Absolute frequency of CD3$^+$ (d), CD4$^+$ (e) and CD8$^+$ T cells (f) within tumors. Data are presented as mean ± s.e.m. (n=4). (g) Representative immunofluorescence of tumors showing CD4$^+$ and CD8$^+$ CAR T cells infiltrating the tumor. Scale bar 50 μm. Statistical significance was calculated *via* two-tailed Student's *t*-test. *P* value: **P* < 0.05; ***P* < 0.01; ****P* < 0.001.

Author Manuscript Author Manuscript Author Manuscript Author Manuscript

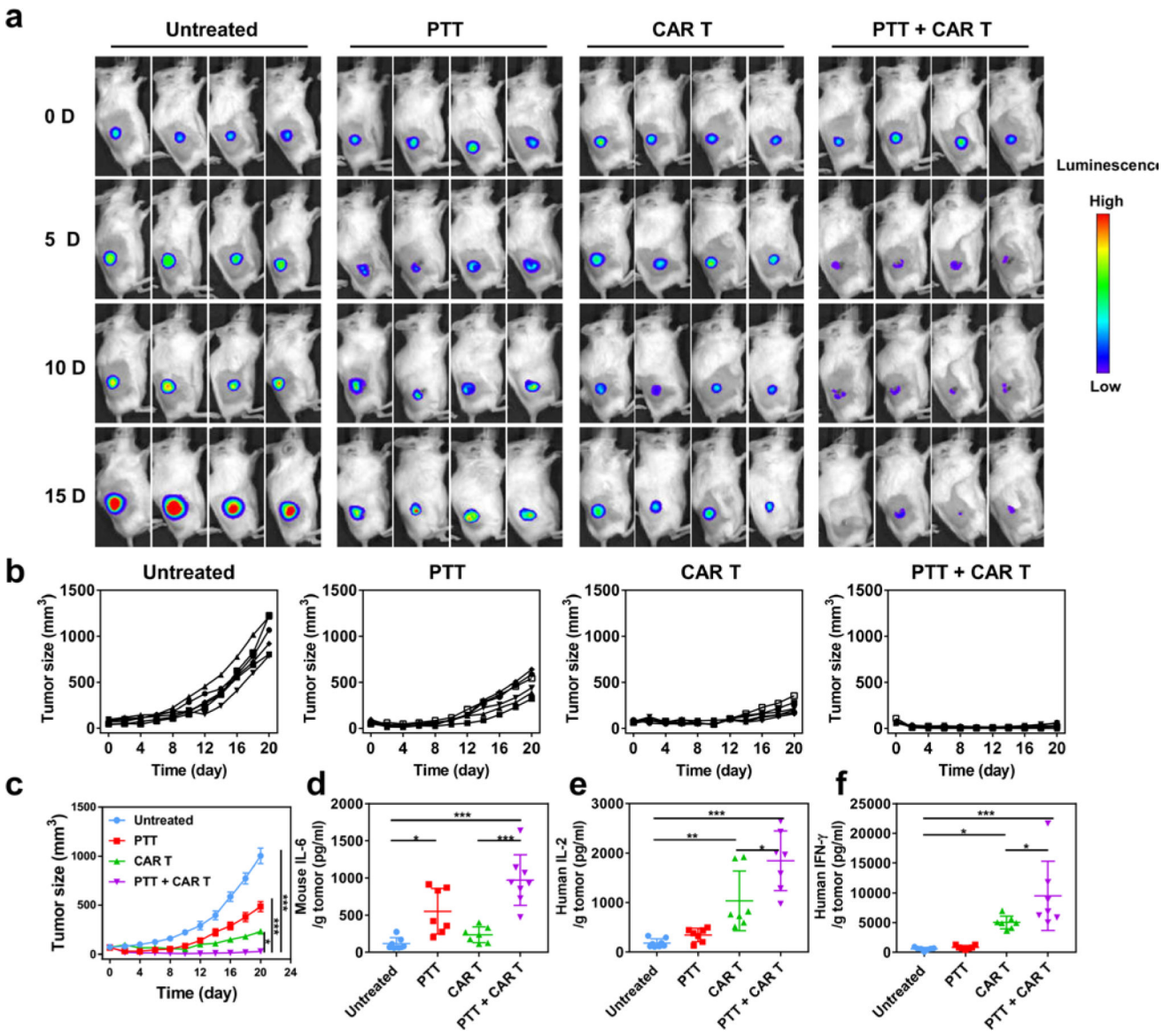

Figure 5. Combined photothermal ablation and adoptive transfer of CAR T cells inhibit the growth of the human melanoma WM115 *in vivo*.

(a) Representative bioluminescence of the WM115 tumors ($n = 4$). (b & c) Individual (b) and average (c) tumor growth kinetics in different groups. Day 0 indicate the day in which treatment was initiated. Data are presented as mean ± s.e.m. ($n = 6$). (d) Murine IL-6 levels detected in the tumors 7 days after the indicated treatments. Data are presented as mean ± s.e.m. ($n = 8$). (e & f) Human IL-2 and IFN-γ levels detected in the tumor 7 days after the indicated treatments. Data are presented as mean ± s.e.m. ($n = 8$). Statistical significance was calculated *via* one-way ANOVA with a Tukey post-hoc test. *P* value: $*P < 0.05$; $**P < 0.01$; $***P < 0.001$.